Angiopoietin-like 4 prevents metastasis through inhibition of vascular permeability and tumor cell motility and invasiveness

Ariane Galaup*†, Aurelie Cazes*†, Sebastien Le Jan*†, Josette Philippe*†, Elisabeth Connault‡, Emmanuelle Le Coz*†, Halima Mekid*†, Lluis M. Mir‡, Paule Opolon‡, Pierre Corvol*†, Catherine Monnot*†, and Stephane Germain*†§¶

*Institut National de la Santé et de la Recherche Médicale, Unit 36, 11 Place Marcelin Berthelot, 75005 Paris, France; †Collège de France, 11 Place Marcelin Berthelot, 75005 Paris, France; ‡Centre National de la Recherche Scientifique, Unité Mixte de Recherche 8121 IGR, 39 Rue Camille Desmoulins, 94805 Villejuif, France; and §Service d'Hématologie Biologique A, AP-HP, Hôpital Européen Georges-Pompidou, 75908 Paris Cedex 15, France

Communicated by Etienne-Emile Baulieu, Collège de France, Le Kremlin-Bicetre, France, October 13, 2006 (received for review January 3, 2006)

Angiopoietin-like 4 (ANGPTL4), a secreted protein of the angiopoietin-like family, is induced by hypoxia in both tumor and endothelial cells as well as in hypoxic perinecrotic areas of numerous cancers. Here, we investigated whether ANGPTL4 might affect tumor growth as well as metastasis. Metastatic 3LL cells were therefore xenografted into control mice and mice in which ANGPTL4 was expressed by using *in vivo* DNA electrotransfer. Whereas primary tumors grew at a similar rate in both groups, 3LL cells metastasized less efficiently to the lungs of mice that expressed ANGPTL4. Fewer 3LL emboli were observed in primary tumors, suggesting that intravasation of 3LL cells was inhibited by ANGPTL4. Furthermore, melanoma B16F0 cells injected into the retro-orbital sinus also metastasized less efficiently in mice expressing ANGPTL4. Although B16F0 cells were observed in lung vessels, they rarely invaded the parenchyma, suggesting that ANGPTL4 affects extravasation. In addition, recombinant B16F0 cells that overexpress ANGPTL4 were generated, showing a lower capacity for *in vitro* migration, invasion, and adhesion than control cells. Expression of ANGPTL4 induced reorganization of the actin cytoskeleton through inhibition of actin stress fiber formation and vinculin localization at focal contacts. Together, these results show that ANGPTL4, through its action on both vascular and tumor compartments, prevents the metastatic process by inhibiting vascular activity as well as tumor cell motility and invasiveness.

angiogenesis | cancer | hypoxia

Understanding the molecular mechanisms that underlie tumor progression, local invasion, and the formation of tumor metastases represents a major challenge in cancer research. Metastasis of tumor cells is the primary cause of death in patients with cancer (1). Cellular mechanisms controlling metastasis affect different tumor cell properties, such as cell locomotion or endothelial cell– and extracellular matrix (ECM)–tumor cell interaction (2, 3). Numerous molecules, including growth factors and their receptors, have been reported to be involved in this process, thereby supporting angiogenesis (4) and/or lymphangiogenesis (5). Among them, angiopoietins that bind to the Tie-2 receptors have been shown to contribute to both angiogenesis and remodeling of lymphatic vessels. Angiopoietin-2-deficient mice form lymphatic vessels but have profound defects in lymphatic vessel remodeling, resulting in chylous ascites and defects in patterning and function of lymphatic vasculature (6), as well as impairment in the responsiveness of endothelial cells to proinflammatory cytokines (7). Also, angiopoietin-3 inhibits pulmonary metastasis by inhibiting tumor angiogenesis (8).

Recently, angiopoietin-like proteins that do not bind to Tie-2 but contain motifs structurally conserved in angiopoietins have been identified. Among them, ANGPTL4, also known as hepatic fibrinogen/angiopoietin-related protein (HFARP) (9), peroxisome proliferator-activated receptor-γ (PPARγ) angiopoietin-related gene (PGAR) (10), or fasting-induced adipose factor (FIAF) (11), is a circulating plasma protein, expressed in the liver, adipose tissue, and placenta (10, 11). ANGPTL4 is up-regulated by fasting, by peroxisome proliferator-activated receptor agonists, associates with lipoproteins (12), and is involved in regulating glucose homeostasis, insulin sensitivity, and lipid metabolism through its capacity to inhibit lipoprotein lipase (12–14).

Previous studies have shown that ANGPTL4 expression is regulated by hypoxia both in endothelial cells (15, 16) and in tumor cells (17). Moreover, ANGPTL4 mRNA is expressed in the perinecrotic areas of various human tumors and is highly up-regulated in epithelial tumor cells from clear-cell renal carcinoma (16). Therefore, several studies have investigated the potential role of ANGPTL4 on angiogenesis. Kim *et al.* showed that ANGPTL4 protects endothelial cells from apoptosis through an endocrine action (9). We have reported an ANGPTL4-proangiogenic response in the chicken chorioallantoic membrane assay (16), whereas Ito *et al.* showed that ANGPTL4 inhibits VEGF-induced vascular leakiness and neoangiogenesis (18). Transgenic mice that express ANGPTL4 in the skin show impaired growth of s.c.-grafted CMT93 murine colorectal tumor cells associated with fewer intratumoral blood vessels (18). These findings suggest that ANGPTL4 exerts multiple biological functions in various contexts, but its potential role in regulating metastases formation has not been investigated yet.

Here, we explored the effects of ANGPTL4 on intravasation, extravasation, and growth of tumor cells in target organs during the metastatic process. We used plasmid DNA electrotransfer into skeletal muscle (19) to release ANGPTL4 into the systemic circulation in two established metastatic models (3LL s.c. injection and B16F0 i.v. injection). Using metastatic 3LL cells, we show that ANGPTL4 prevents metastasis through inhibition of tumor cell intravasation from the primary tumor to lymphatic or blood vessels without affecting angiogenesis or lymphangiogenesis. We also show that ANGPTL4 inhibits extravasation of B16F0 cells from the circulation to lungs, as well as vascular permeability. In addition *in vitro*, we used stably transfected melanoma B16F0 cell lines expressing and secreting ANGPTL4, thereby demonstrating a direct autocrine effect of ANGPTL4 on B16F0 tumor cells through inhibition of migration, invasion, adhesion, and cytoskeleton reorganization.

Together, these results show that ANGPTL4, through its action on both vascular and tumor compartments, is able to prevent the

Author contributions: A.G., P.C., and S.G. designed research; A.G., A.C., S.L.J., J.P., E.C., E.L.C., H.M., L.M.M., P.O., C.M., and S.G. performed research; L.M.M. contributed new reagents/analytic tools; A.G., A.C., S.L.J., J.P., P.O., P.C., C.M., and S.G. analyzed data; and A.G. and S.G. wrote the paper.

The authors declare no conflict of interest.

Abbreviations: ANGPTL4, angiopoietin-like 4; TG, triglycerides; VP, vascular permeability; ECM, extracellular matrix.

¶To whom correspondence should be addressed. E-mail: stephane.germain@college-de-france.fr.

© 2006 by The National Academy of Sciences of the USA

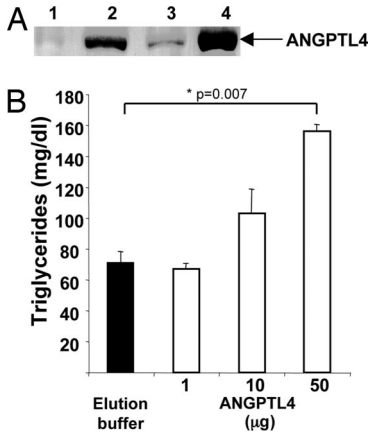

Fig. 1. *In vivo angptl4* gene transfer by electrotransfer. Western blot analysis of ANGPTL4-mycHis protein detected by c-myc antibody. (*A*) Sera from mice electrotransferred with control plasmid (week 2, lane 1) or with ANGPTL4 (week 2, lane 2 and week 6, lane 3), and from mice injected with 1 μg of recombinant ANGPTL4 (lane 4) were analyzed. (*B*) Assessment of plasma TG from mice injected 30 min before with control buffer or recombinant ANGPTL4 (1, 10, or 50 μg), by enzymatic reaction.

metastastic process through inhibition of vascular activity as well as tumor cell motility and invasiveness.

Results

***In Vivo* ANGPTL4 Gene Transfer by Electrotransfer.** We first studied whether pcDNA3.1-ANGPTL4-mycHis plasmid injection in *Tibialis cranialis* combined with electrotransfer allowed a stable and a long-term production of secreted ANGPTL4 protein. As shown in Fig. 1*A*, ANGPTL4 was detected by Western blot 2 and 6 weeks after electrotransfer (lane 2 and 3), in sera from mice injected with pcDNA3.1-ANGPTL4-mycHis plasmid as compared with control mice injected with pcDNA3.1-mycHis empty plasmid (lane 1). Moreover, as shown comparing lanes 2 (2 weeks after ANGPTL4 electrotransfer) and 4 (injection of 1 μg of the recombinant ANGPTL4), electrotransfer allowed the production of low levels of ANGPTL4 (<1 μg). To determine whether this tagged version of ANGPTL4 was active *in vivo*, we also determined the level of TG in plasma of mice injected with various doses of recombinant ANGPTL4. Systemic injection of 50 μg of purified recombinant ANGPTL4 significantly increases plasma TG as compared with the injection of elution buffer (156 ± 3 versus 71 ± 5 mg/dl, $P = 0.007$). Lower levels of circulating protein (10 and 1 μg) as well as the amount of electrotransferred protein used in this study did not significantly modify plasma TG (Fig. 1*B*). Then, to avoid any confounding role of ANGPTL4 on TG, we here study the effect of sustained but low levels of ANGPTL4 obtained after electrotransfer (<1 μg) on tumor growth and metastasis.

ANGPTL4 Inhibits 3LL Tumor Cell Intravasation, Invasion of Lymph Nodes, and Lung Metastases. Murine 3LL cells, which mimic metastasis from primary tumor to lung, were s.c. injected in mice to evaluate whether circulating ANGPTL4 might affect tumor growth as well as the metastatic process. Four weeks after 3LL cell injection, no significant difference in primary tumor volumes or in the number of intratumoral blood and lymphatic vessels was observed in ANGPTL4 expressing mice compared with control mice (data not shown). In contrast, as shown in Fig. 2*A*, the incidence of emboli, defined as the presence of tumor cells within vessels inside tumors or at its vinicity (see arrows), was decreased in ANGPTL4 mice ($14.6 \pm 1.4\%$ versus $56.3 \pm 4.5\%$, $P = 0.04$). This phenomenon correlated with the inhibition of local invasion to lymph nodes (Fig. 2*B*) and distant metastases formation to lungs (Fig. 2*C*) observed in ANGPTL4 mice. Indeed, a decreased number of invaded lymph nodes was observed in ANGPTL4 mice compared with control mice all along the course of the study (0 of 5 invaded lymph nodes versus 4 of 5 at week 2 and 3 of 5 invaded lymph nodes versus 5 of 5 at week 4) (Fig. 2*B Left*). In addition, mean volume of metastatic lymph nodes was also diminished in ANGPTL4 mice compared with control (19.8 ± 9.8 versus 42.0 ± 5.0 mm^3 at week 3 and 76.8 ± 8.4 versus 110.4 ± 17.2 mm^3 at week 4, $P < 0.05$) (Fig. 2*B*).

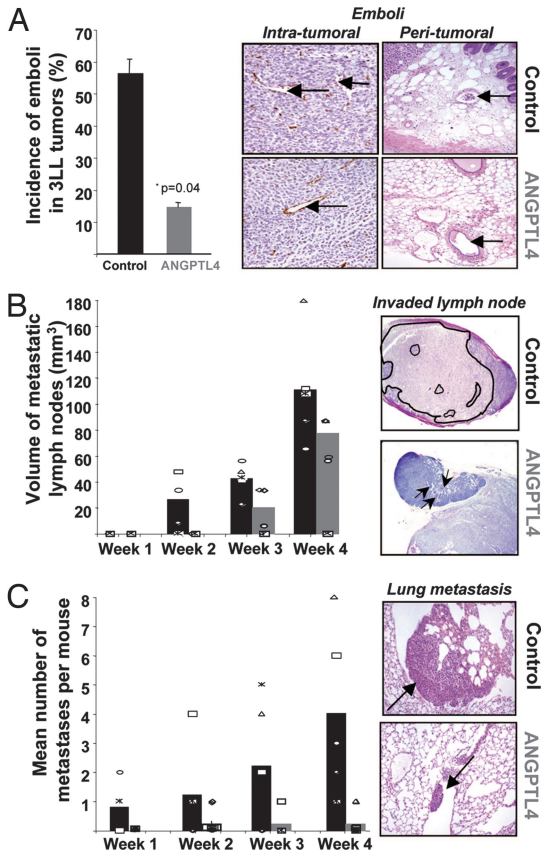

Fig. 2. ANGPTL4 inhibits 3LL tumor cell intravasation, invasion of lymph nodes, and lung metastases. Two weeks after muscle electroporation, C57BL/6 mice were s.c. implanted with 3LL cells. One, two, three, and four weeks after implantation, tumors, lymph nodes, and lungs were removed and stained by using HES and anti-CD34 immunohistochemistry. Invading tumor cells (emboli) were mainly observed in control mice (intratumor vessels, peritumor vessels, see arrows) (*A*). The number and the volume of metastatic lymph nodes (*B*) as well as the number of 3LL micrometastases in lungs (*C Left*) were quantified in sections from ANGPTL4 mice compared with control mice each week after injection. Typical views of invaded lymph nodes (*B Right*; see the tumor area surrounded in black in control mouse versus diffuse tumor cells shown by arrows in ANGPTL4 mice) and lung metastases (*C Right*) are shown.

As for distant invasion, incidence of lung metastases formation was lower in ANGPTL4 versus control group from week 1 (0 of 5 versus 3 of 5 mice) to week 4 (1 of 5 versus 5 of 5 mice). Mean number of metastases was also diminished (4.0 ± 1.3 versus 0.2 ± 0.2 in ANGPTL4 mice, $P = 0.016$; Fig. 2*C*). These data therefore suggest that ANGPTL4 inhibits intravasation of metastatic 3LL cells from the primary tumor, leading to fewer local and distant metastases.

ANGPTL4 Inhibits Extravasation and Macrometastases Formation. To evaluate any role of ANGPTL4 on the extravasation step of tumor cells, we also used B16F0 melanoma cells, which when i.v. injected, survive, extravasate, divide, and form lung metastases. B16F0 cells were i.v. injected into ANGPTL4 electrotransferred or control

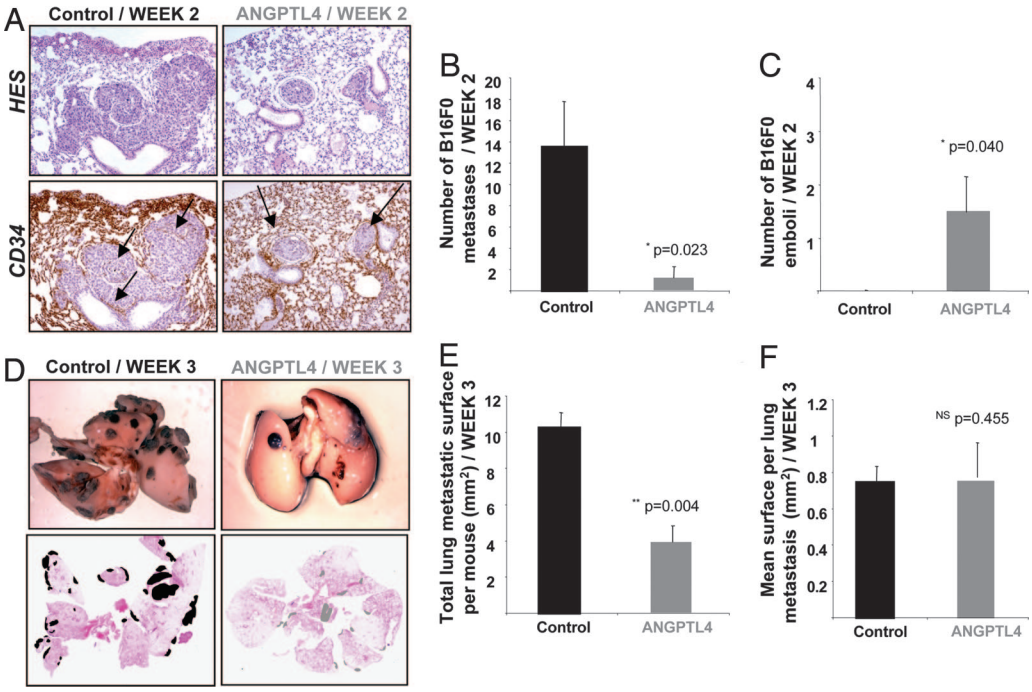

Fig. 3. In the B16F0 model, ANGPTL4 inhibits extravasation of tumor cells and macrometastases number. B16F0 cells were injected i.v. into C57BL/6 mice 2 weeks after ANGPTL4 electroporation, and mice were killed either 2 or 3 weeks later. At week 2, tumor islets were observed in lungs by staining sections with HES (*A Upper*) and anti-CD34 (*A Lower*), allowing discrimination of C57BL/6 micrometastases implanted in the lung parenchyma from intravascular emboli. Left panel, arrows indicate residual vascular walls associated with tumor cell extravasation in control lung. Right panel, arrows show intact vessels enclosing localized nodules (emboli) in lungs from ANGPTL4 mice (*A*). Quantification of micrometastases invaded the parenchyma of the lung (*B*) and localized emboli (*C*). Typical views of lungs presenting macroscopic metastases at week 3 (*D Upper*). For each mouse, quantification of total metastatic area (*E*) and mean surface area per macrometastasis (*F*) was performed by using scanned images of HES-stained lung sections (*D Lower*).

mice, which were then killed 2 weeks after injection. Then, lungs were examined for tumor islets, and tumor cells that had invaded into the lung parenchyma (micrometastases) were distinguished from tumor cells that remained within intact vessel lumens (emboli) using HES and CD34-staining (Fig. 3*A*). In the control group, many micrometastases were established (13.5 ± 4.2) and no intravascular tumor cells, i.e., emboli, remained. In contrast, 1.5 ± 1.2 micrometastases and 1.5 ± 1.4 emboli were observed in the ANGPTL4 group ($P = 0.023$; Fig. 3 *B* and *C*), suggesting that ANGPTL4 inhibits B16F0 tumor cells extravasation.

To appreciate the development of large metastases, B16F0 cells were i.v. injected in ANGPTL4 or control mice, and mice were killed after 3 weeks. Macroscopically, examination of lungs showed a reduced number of macrometastases in ANGPTL4-expressing mice (Fig. 3*D Upper*). Quantification from HES-stained lung sections (Fig. 3*D Lower*) showed that the total tumor surface in ANGPTL4 mice was decreased (3.9 ± 0.9 mm^2) compared with control mice (12.0 ± 0.8 mm^2, $P = 0.004$) (Fig. 3*E*). As shown in Fig. 3*F*, quantification of the mean tumor surface per macrometastasis revealed no significant difference between both groups (0.8 ± 0.2 mm^2 versus 0.7 ± 0.1 mm^2, $P = 0.455$). These data suggest that whereas ANGPTL4 inhibits metastases seeding, it does not affect proliferation when implanted into the target organ.

Inhibition of Histamine-Induced Vascular Permeability by ANGPTL4. Because metastasis depends on tumor–endothelial cell interaction and vascular permeability (VP), we investigated whether ANGPTL4 inhibition of intravasation and extravasation might be, at least in part, explained by a decrease in VP, as previously shown in transgenic mice (18). Miles assays performed in response to injection of 1 or 10 nM histamine were used to induce VP in ANGPTL4 and control mice. As shown in Fig. 4, vascular permeability induced by 10 nM histamine was significantly lower in ANGPTL4 mice compared with control mice (56.3 ± 2.7 versus 91.8 ± 0.9 ng of Evans blue per milligram of fresh tissue, $P = 0.002$).

ANGPTL4 Inhibits Tumor Cell Motility and Invasiveness. To determine whether ANGPTL4 might directly modify tumor cell behavior, we stably transfected B16F0 cells either with an ANGPTL4 expressing plasmid (ANGPTL4 cells) or an empty vector (control cells). As shown in Fig. 5*A*, and in accordance with previous reports (20), ANGPTL4 was produced in both full length (50 kDa) and in truncated form (35 kDa) into cultured medium. Three clones showing three different levels of expression, (-Low, -Medium, or -High), were used for *in vitro* characterization. No significant difference was observed in proliferation, cell viability, cell cycle, or apoptosis between control cells and ANGPTL4 cells (data not shown). However, whatever the expression level, adhesion to various supports such as BSA, fibronectin, laminin, or vitronectin was significantly inhibited in cells expressing ANGPTL4 compared with control cells (inhibition from 17.0% to 35.0% for B16F0/ANGPTL4-High; Fig. 5*B*).

The effect of ANGPTL4 expression on tumor cell motility was then evaluated by using a Boyden chamber assay. As shown in Fig. 5*C*, migration of ANGPTL4 cells was significantly reduced com-

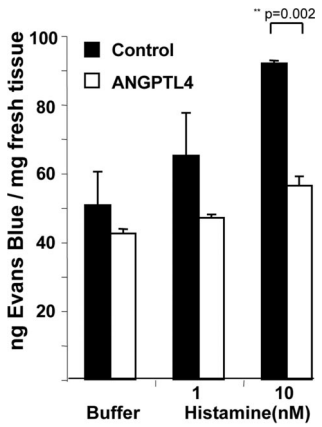

Fig. 4. Inhibition of histamine-induced vascular permeability by ANGPTL4. VP was evaluated by performing a Miles assay induced by histamine in *nude* mice electrotransferred with ANGPTL4 or control plasmid. Spectrophotometric analysis of vascular leakiness with Evans blue dye was performed. For each group, extravasation of dye after injection of histamine (1 nM, 10 nM) was compared with extravasation of dye after injection of PBS. Mean nanograms of Evans blue per milligram of fresh tissue are represented ± SEM.

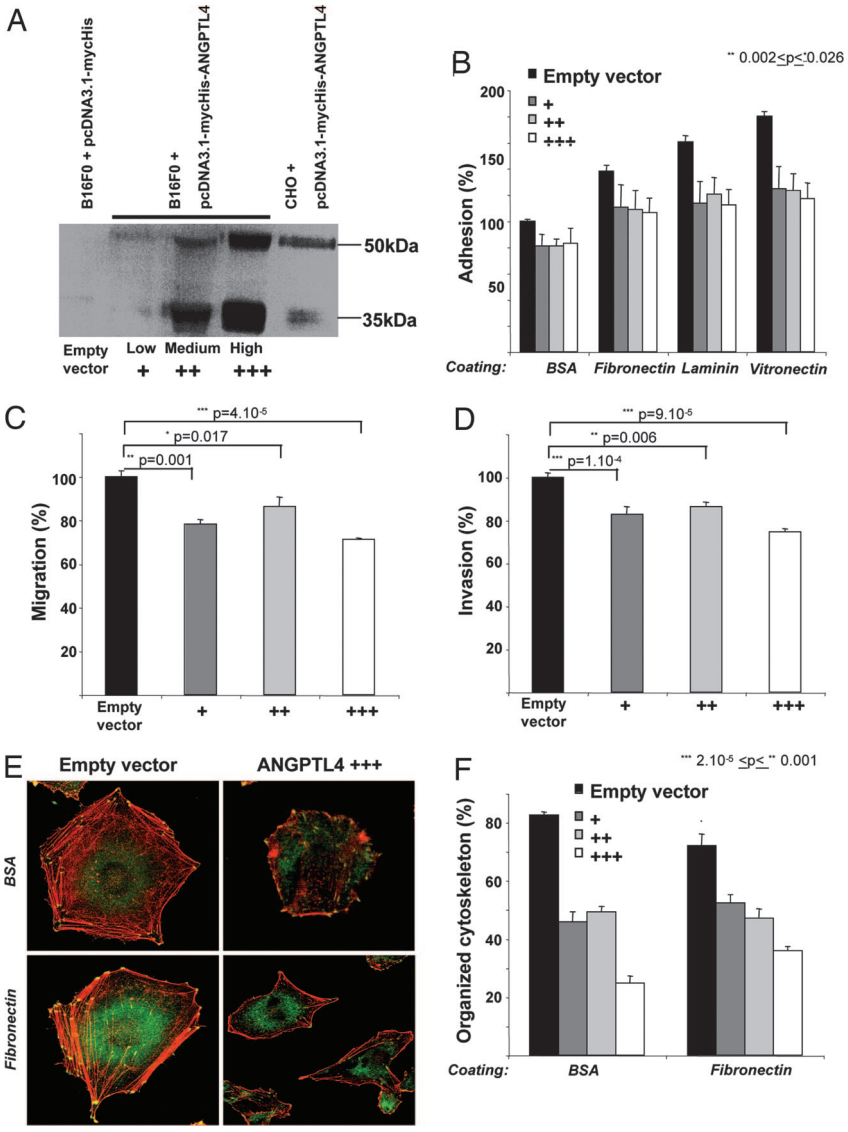

Fig. 5. *In vitro* characterization of the overexpression of ANGPTL4 in tumor cells. Western blot analysis of ANGPTL4-mycHIS protein secreted by stably transfected B16F0 clones (B16F0/ANGPTL4-Low, -Medium, or -High) compared with control cells (B16F0/Empty vector as negative control and CHO/ANGPTL4 as positive control (16) and detected by c-myc antibody (*A*). Alteration of tumor cell adhesion, motility, and invasiveness by ANGPTL4. ''Adhesion assay'': 5×10^4 stained B16F0 cells expressing ANGPTL4 or control cells were plated on BSA, fibronectin, laminin, or vitronectin for 1 h, and fluorescence was measured (*B*). ''Boyden chamber assay'': 1×10^5 stained cells expressing ANGPTL4 or control cells were seeded in transwells with polycarbonate membrane plates. Migration on a fibronectin coating (*C*) or invasion through a Matrigel barrier (*D*) was assessed by measuring fluorescence after 6 h. ANGPTL4 modifies cytoskeleton organization. Cytoskeleton organization of B16F0 ANGPTL4 cells or control cells was evaluated by fluorescence detection of polymerized actin fibers (red) and vinculin (green) (*E*). Quantification was performed by determining the percentage of cells showing an organized cytoskeleton, i.e., polymerized actin stress fibers (red) and vinculin focal adhesion contacts (green) in control and ANGPTL4 cells (*F*).

pared with control cells (inhibition of 28.5 ± 0.6% for B16F0/ANGPTL4-High, $P = 4 \times 10^{-5}$). Furthermore, invasion through Matrigel was decreased in ANGPTL4 cells compared with the control cells (inhibition of 25.4 ± 1.4% for B16F0/ANGPTL4-High, $P = 9 \times 10^{-5}$; Fig. 5*D*). Together, these experiments indicate that ANGPTL4 inhibits tumor cell motility, adhesion, and invasiveness.

ANGPTL4 Modifies Cytoskeleton Organization. The inhibitory effect of ANGPTL4 in cell motility might suggest that ANGPTL4 affects cell spreading and cytoskeleton organization. As shown in Fig. 5*E*, B16F0 control cells display a classical well-organized cytoskeleton with many polymerized actin stress fibers (red staining) and attached cells via vinculin focal adhesions (green staining). In comparison, the cytoskeleton of ANGPTL4 cells lacked stress fibers and showed a diffused vinculin-localization pattern. Quantification of cells showing a well organized cytoskeleton on BSA or fibronectin confirmed that ANGPTL4 inhibits cell spreading and cytoskeleton organization even in low expressing cells (Fig. 5*F*). On fibronectin, well organized cytoskeletons were observed in 72.1 ± 9.2% of B16F0 control cells versus 52.4 ± 6.4% of B16F0/ANGPTL4-Low cells ($P = 0.001$), 47.1 ± 7.5% of B16F0/ANGPTL4-Medium cells ($P = 4 \times 10^{-4}$), and 36.1 ± 3.1% of B16F0/ANGPTL4-High cells ($P = 4 \times 10^{-7}$).

Discussion

In the present study, we provide evidence that ANGPTL4 inhibits metastasis, and we identify the steps on which ANGPTL4 may exert its action. Using DNA electrotransfer, we were able to produce low (below circulating values obtained by injecting 1 μg of purified protein) and sustained levels of circulating ANGPTL4 in mice. This method was chosen to avoid any confounding role of ANGPTL4 on metabolism because, as previously published by others (12, 13, 21), we show that only higher levels (>50 μg) of ANGPTL4 protein are able to acutely induce increase of TG in the plasma.

First, we showed that ANGPTL4 inhibits metastasis by modulating intravasation of tumor cells. This phenomenon represents the first step of the metastatic process and implies the presence of blood vessels and lymphatics within and around the tumor as well as interactions between tumor and endothelial cells. Unlike angiopoietins and other members of the angiopoietin-like family that have been shown to regulate angiogenesis, namely ANGPTL1 (22, 23), ANGPTL2 (23), and ANGPTL3 (24), ANGPTL4 did not affect lymph or blood vessel density of primary Lewis lung carcinoma (3LL) tumors but decreased their *in vivo* intravasating potential.

Then, after entry into the circulation and before formation of metastases into target organs, tumor cell extravasation is required. We show here that ANGPTL4 inhibits the extravasation step.

Indeed, the number of B16F0 micrometastases within the lung parenchyma is markedly decreased in mice that express ANGPTL4 compared with control mice. Instead of implanted metastases, emboli mostly remained intravascular in the ANGPTL4-electrotransferred mice. In addition, micrometastases that developed as macroscopic tumors were also fewer in ANGPTL4 mice, but their size was not significantly different, suggesting that, whereas B16F0/ANGPTL4 cells deposits were more rarely observed in the lung, their growth into the target organ was not affected. Interestingly, the overall survival of mice was not affected (data not shown), suggesting that the mice died from development of the primary tumor itself, which was not affected by ANGPTL4 expression, or that despite the fact that fewer metastases were able to develop, these were sufficient to induce death of the mice.

The mechanisms of the antimetastatic effect of ANGPTL4 were further investigated. First, alterations of vascular properties were shown to be induced by ANGPTL4. Indeed, we showed that ANGPTL4 inhibits histamine-induced permeability, in accordance with a previous study that reported inhibition of VEGF-induced vessel leakiness by ANGPTL4 (18). This property has also been observed with angiopoietin 1 (25). These data suggest that endothelial cells may be a target of ANGPTL4, an observation which is consistent with previous studies (9, 18) and our unpublished observations.

In addition, we showed that ANGPTL4 also acts on tumor cells. Using recombinant murine melanoma B16F0/ANGPTL4 cells stably secreting ANGPTL4 at various levels, we showed inhibition of tumor cell migration, invasion, and adhesion compared with B16F0 control cells. We further showed that ANGPTL4 affects cytoskeleton organization and focal adhesion formation. Disruption of actin stress fibers and focal adhesions, structures that link the cytoskeleton to integrins, and the ECM induces decreased adhesion, traction, and consecutively, directional invasion and migration. The inhibition of cytoskeleton organization was more potent in highly expressing cells compared with medium or low expressing cells, whereas inhibition of migration, invasion, and adhesion was comparable in these three cell lines, suggesting that low levels of ANGPTL4 are sufficient to confer the observed inhibition *in vitro*.

The intravasation and extravasation steps during the metastasis process are regulated by a variety of molecules, including cell–cell and cell–ECM receptors, proteolytic enzymes involved in the breakdown of the basal membrane and invasion of vascular channels and organs, motility factors allowing migration through tissues, and receptors mediating organ specific invasion. E-cadherin and its associated catenin complex (26), as well as Connexin 26, through heterologous gap junction formation with endothelial cells (27), play a crucial role in intravasation and extravasation of tumor cells. The potential modulation of homotypic and heterotypic cell interactions by ANGPTL4 therefore requires further investigations. Finally, integrins are a class of ECM receptors that trigger specific intracellular pathways to initiate distinct cellular responses, such as actin cytoskeleton assembly or cell adhesion and migration, properties that are modulated by ANGPTL4 in the present study. Among the integrins, β1 integrin is crucial for adhesion, spreading, and motility of tumor cells (28), and it plays a critical role in CXCR4-mediated B16 tumor cell metastasis (29). Whether ANGPTL4 effect on tumor cells is mediated through integrin activity is presently under study. Together, whereas a hypoxic environment tends to favor tumor cell spread, our results suggest that ANGPTL4, synthesized in this context, conditions tumor microenvironment and in turn affects vascular activity as well as tumor cell motility and invasiveness and participates in the inhibition of metastases. Therefore, this study suggests that ANGPTL4 might be a good therapeutic inhibitor of metastases. Nevertheless, further *in vivo* and *in vitro* experiments will be necessary to decipher its full mechanism of action.

Materials and Methods

Cell Culture. Lewis lung carcinoma 3LL cells were cultured with RPMI medium supplemented with 10% FCS and 1 mM L-glutamine (Invitrogen). B16F0/ANGPTL4 cell lines were established by transfecting B16F0 cells with the full-length human ANGPTL4 cDNA in pcDNA3.1mycHis (Invitrogen) and by selecting three stably transfected clones (with -Low; -Medium or -High expression of ANGPTL4-mycHis) with geniticin (GIBCO/BRL). A B16F0/Empty vector cell line was established by transfection with pcDNA3.1mycHis (Invitrogen) and was used as control for the *in vitro* study. Cells were maintained in MEM-Glutamax medium (Invitrogen) supplemented with 10% FCS.

Electrotransfer. Twenty micrograms of DNA in 20 μl of sterile saline was injected into each tibialis cranialis of 8-week-old mice. One pulse of 800 V/cm and 100 μs of duration followed 1 s later by a pulse of 80 V/cm and 400 ms of duration (19) were delivered by a Cliniporator device (IGEA). Seven independent experiments were performed with two randomized groups (n = 5–10 mice per group). The control group received pcDNA3.1-mycHis plasmid injections, and the ANGPTL4 group was injected with pcDNA3.1-ANGPTL4-mycHis plasmid. Electrotransfer was performed 2 weeks before all *in vivo* experiments (3LL model, n = 3; B16F0 model, n = 2; and Miles assay, n = 2).

Metastatic Models. Experiments were performed with 10-week-old C57BL/6 female mice. Cultured 3LL and B16F0 cells were resuspended in PBS at 1×10^7 cells per ml. Tumor 3LL cells (200 μl) were injected s.c. in ANGPTL4 and control groups. Sera, tumors, lymph nodes, and lungs were collected weekly from control mice (n = 5) and ANGPTL4 electrotransferred mice (n = 5) during 4 weeks for expression and histology studies. As for B16F0 cells, mice from ANGPTL4 and control groups received one 50-μl i.v. injection of cells via the retro-orbital sinus. Lungs were collected 2 or 3 weeks after injection of tumor cells.

Immunohistochemistry and Image Analysis. The different specimens (primary tumors, lymph nodes, and lungs for the 3LL model and lungs for the B16F0 model) from all of the mice studied in five experiments were fixed in Finefix (Milestone Medical), and then paraffin sections (4 μm thick) and hematoxylin-eosin-saffranin (HES) slides were prepared. For immunohistochemistry, tumor and lung sections were incubated with rat primary antibody raised against mouse CD34 (clone MEC 14.7; Hycult Biotechnology). All of the sections were analyzed by using a Zeiss Axiophot microscope and a SensiCam PCO digital camera. Representative views were taken at a magnification of 100×.

In the 3LL model, CD34- and HES-stained slides of the maximal sections of the primary tumors, the lymph nodes, and the lungs obtained from 40 mice (control or ANGPTL4 mice killed at weeks 1, 2, 3, and 4) were analyzed by two independent operators. Emboli (tumor cells invading lumen of the vessels) were counted inside and at the vicinity of the primary tumors. The incidence, the volume of the metastatic lymph nodes, and the number of 3LL micrometastases in lungs were also determined.

CD34- and HES-stained slides of the lungs obtained from the 12 mice i.v. injected with B16F0 and killed 2 weeks after injection were observed by two independent operators to distinguish and count micrometastases that had implanted into the lung parenchyma from emboli that had remained intravascular.

The lungs of 13 mice i.v. injected with B16F0 and removed 3 weeks after injection were analyzed for the assessment of the development of macrometastases. HES-stained sections of these lungs were digitized with a slide scanner (SuperCoolscan 8000 ED; Nikon). As previously published, a dedicated script was implemented to the PIXCYT software (30) to determine the total metastatic surface per mouse and the mean surface per metastasis.

Analysis of 57 metastases for the control group and 21 metastases for the ANGPTL4 group was performed by two different operators.

Miles Assay. Female 10-week-old athymic *nude* mice from ANGPTL4 and control groups were anesthetized, and 200 μl of 1% Evans blue dye (Sigma) was injected into tail vein. Five minutes after the dye injection, 20 μl of histamine (1 and 10 nM) or PBS was intradermally injected in the side of the mouse back. Skin surrounding the injected sites was removed 20 min later and weighed, and the blue dye was extracted from skin with formamide during 48 h at 37°C. The amount of extravasated dye was measured with a spectrophotometer (610 nm). For each group, leakiness was reported in nanograms of Evans blue per milligram of fresh tissue. Values shown are the mean ± SEM ($n = 3$ mice per condition).

Western Blot Analysis. Blood samples were collected 2 and 6 weeks after electrotransfer from ANGPTL4 and control mice. As control and semiquantitative method, 1 μg of recombinant ANGPTL4-mycHis protein was injected into the tail vein of 10-week-old C57BL/6 female mice, and blood samples were collected 30 min later. For *in vitro* analysis, B16F0/Empty vector and B16F0/ANGPTL4-Low, -Medium, or -High cells were plated into T75-flask in serum-free medium. Supernatants were collected after 48 h and concentrated with Amicon Ultra filters (Millipore). Supernatant of CHO cells expressing ANGPTL4 (16) was included as control. Western blots were probed with antibody directed against c-myc tag (clone 9E10; Roche) and detected with a biotin-streptavidin system.

Enzymatic Determination of Triglycerides in Mice Blood. Recombinant ANGPTL4-mycHis protein was purified from stably transfected CHO cells by affinity chromatography (Cobalt affinity column Talon; BD Biosciences). Then, 200 μl containing 0, 1, 10, or 50 μg of purified ANGPTL4 was injected into tail vein of 10-week-old C57BL/6 female mice ($n = 12$). Blood samples were collected 30 min after injection, and plasma triglycerides (TG) were measured by enzymatic reaction (TG PAP 150 kit; Biomerieux). Values shown are the mean ± SEM ($n = 3$ mice per condition).

Adhesion Assay. Culture plates (24-well) were coated with BSA, fibronectin, laminin, or vitronectin (10 μg/ml) for 30 min at 37°C and washed and blocked with PBS/1% BSA for 30 min at 37°C. B16F0/Empty vector and B16F0/ANGPTL4-Low, -Medium, or -High cells were prestained with calcein AM (5 μg/ml; Molecular Probes) for 30 min at 37°C. Stained cells (5×10^4) were plated and allowed to adhere for 1 h at 37°C. Nonadherent cells were washed away three times with PBS, and fluorescence of the cells was measured by using a computer-based fluorescence reader (Fusion; Packard). All conditions were performed in triplicate. Values shown are the mean ± SEM of three independent experiments.

Migration and Invasion Assays in Boyden Chambers. Migration and invasion assays were performed by using HTS Fluoroblok 24-well chambers containing filters with 8-μm pore size (BD Biosciences). For the migration assay, filters were precoated on the lower side with fibronectin (10 μg/ml). For the invasion assay, filters were precoated on the upper side with Matrigel (20 μg per well; BD Biosciences). Serum-free conditioned medium from NIH 3T3 cells cultured for 18 h was placed on the lower compartment of the chamber. B16F0/Empty vector and B16F0/ANGPTL4-Low, -Medium, or -High cells were prestained with calcein AM (5 μg/ml; Molecular Probes) for 30 min at 37°C, and 10^5 cells were seeded in serum-free MEM on the upper compartment of the chambers for 6 h at 37°C. The fluorescence of the cells in the lower side of the filter was measured in the wells by using a computer-based fluorescence reader (Fusion; Packard). All conditions were performed three times in triplicate. Values shown are the mean ± SEM.

Immunofluorescence Assays. Glass coverslips were coated with fibronectin (10 μg/ml) or BSA (10 μg/ml) for 1 h at 37°C then washed and blocked with PBS/1% BSA for 30 min. Control and ANGPTL4 cells were added and cultured for 48 h in complete medium. Actin was visualized with rhodamine-phalloidin (Molecular Probes), and vinculin was detected with clone H20.1 (Sigma). The cytoskeleton reorganization was evaluated as percentage of spread cells with actin stress-fibers and vinculin focal adhesions after adhesion of control and ANGPTL4 cells. For each condition (fibronectin or BSA), >100 cells were considered by two different evaluators, and the experiments were independently performed three times. Values shown are the mean ± SEM.

Statistical Analysis. Statistical analysis was performed and P values were calculated according to Student's t test. Significant differences were accepted for $P < 0.05$.

We thank Eric Etienne for the help provided for confocal microscopy, Steven Suchting for critical reading of the manuscript, and le Service Commun d'Expérimentation Animale (SCEA) for animal care. A.G. is supported by a grant from la Fondation Lefoulon Delalande/Institut de France. This work emanates from the European FP6 project European Vascular Genomics Network (Contract LSHM-CT-2003-503254). S.G. is supported by grants from la Fondation de France and Canceropole-PACA ACI 2004. This work was supported in part by a grant from Novartis.

1. Fidler IJ (1999) *Cancer Chemother Pharmacol* 43(Suppl):S3–S10.
2. Crissman JD, Hatfield JS, Menter DG, Sloane B, Honn KV (1988) *Cancer Res* 48:4065–4072.
3. Hynes RO (2002) *Cell* 110:673–687.
4. Carmeliet P (2003) *Nat Med* 9:653–660.
5. Achen MG, McColl BK, Stacker SA (2005) *Cancer Cell* 7:121–127.
6. Gale NW, Thurston G, Hackett SF, Renard R, Wang Q, McClain J, Martin C, Witte C, Witte MH, Jackson D, Suri C, Campochiaro PA, Wiegand SJ, Yancopoulos GD (2002) *Dev Cell* 3:411–423.
7. Fiedler U, Reiss Y, Scharpfenecker M, Grunow V, Koidl S, Thurston G, Gale NW, Witzenrath M, Rosseau S, Suttorp N, Sobke A, Herrmann M, Preissner KT, Vajkoczy P, Augustin HG (2006) *Nat Med* 12:235–239.
8. Xu Y, Liu YJ, Yu Q (2004) *Cancer Res* 64:6119–6126.
9. Kim I, Kim HG, Kim H, Kim HH, Park SK, Uhm CS, Lee ZH, Koh GY (2000) *Biochem J* 346:603–610.
10. Yoon JC, Chickering TW, Rosen ED, Dussault B, Qin Y, Soukas A, Friedman JM, Holmes WE, Spiegelman BM (2000) *Mol Cell Biol* 20:5343–5349.
11. Kersten S, Mandard S, Tan NS, Escher P, Metzger D, Chambon P, Gonzalez FJ, Desvergne B, Wahli W (2000) *J Biol Chem* 275:28488–28493.
12. Mandard S, Zandbergen F, van Straten E, Wahli W, Kuipers F, Muller M, Kersten S (2006) *J Biol Chem* 281:934–944.
13. Yoshida K, Shimizugawa T, Ono M, Furukawa H (2002) *J Lipid Res* 43:1770–1772.
14. Xu A, Lam MC, Chan KW, Wang Y, Zhang J, Hoo RL, Xu JY, Chen B, Chow WS, Tso AW, Lam KS (2005) *Proc Natl Acad Sci USA* 102:6086–6091.
15. Le Jan S, Le Meur N, Philippe J, Le Cunff M, Leger J, Corvol P, Germain S (2006) *FEBS Lett* 12:3395–4400.
16. Le Jan S, Amy C, Cazes A, Monnot C, Lamande N, Favier J, Philippe J, Sibony M, Gasc JM, Corvol P, Germain S (2003) *Am J Pathol* 162:1521–1528.
17. Lal A, Peters H, St Croix B, Haroon ZA, Dewhirst MW, Strausberg RL, Kaanders JH, van der Kogel AJ, Riggins GJ (2001) *J Natl Cancer Inst* 93:1337–1343.
18. Ito Y, Oike Y, Yasunaga K, Hamada K, Miyata K, Matsumoto S, Sugano S, Tanihara H, Masuho Y, Suda T (2003) *Cancer Res* 63:6651–6657.
19. Satkauskas S, Bureau MF, Puc M, Mahfoudi A, Scherman D, Miklavcic D, Mir LM (2002) *Mol Ther* 5:133–140.
20. Ge H, Yang G, Huang L, Motola DL, Pourbahrami T, Li C (2004) *J Biol Chem* 279:2038–2045.
21. Koster A, Chao YB, Mosior M, Ford A, Gonzalez-DeWhitt PA, Hale JE, Li D, Qiu Y, Fraser CC, Yang DD, Heuer JG, Jaskunas SR, Eacho P (2005) *Endocrinology* 146:4943–4950.
22. Dhanabal M, LaRochelle WJ, Jeffers M, Herrmann J, Rastelli L, McDonald WF, Chillakuru RA, Yang M, Boldog FL, Padigaru M, McQueeney KD, Wu F, Minskoff SA, Shimkets RA, Lichenstein HS (2002) *Cancer Res* 62:3834–3841.
23. Kubota Y, Oike Y, Satoh S, Tabata Y, Niikura Y, Morisada T, Akao M, Urano T, Ito Y, Miyamoto T, Nagai N, Koh GY, Watanabe S, Suda T (2005) *Proc Natl Acad Sci USA* 102:13502–13507.
24. Camenisch G, Pisabarro MT, Sherman D, Kowalski J, Nagel M, Hass P, Xie MH, Gurney A, Bodary S, Liang XH, Clark K, Beresini M, Ferrara N, Gerber HP (2002) *J Biol Chem* 277:17281–17290.
25. Thurston G, Suri C, Smith K, McClain J, Sato TN, Yancopoulos GD, McDonald DM (1999) *Science* 286:2511–2514.
26. Beavon IR (1999) *Mol Pathol* 52:179–188.
27. Ito A, Katoh F, Kataoka TR, Okada M, Tsubota N, Asada H, Yoshikawa K, Maeda S, Kitamura Y, Yamasaki H, Nojima H (2000) *J Clin Invest* 105:1189–1197.
28. Hegerfeldt Y, Tusch M, Brocker EB, Friedl P (2002) *Cancer Res* 62:2125–2130.
29. Cardones AR, Murakami T, Hwang ST (2003) *Cancer Res* 63:6751–6757.
30. Elie N, Plancoulaine B, Signolle JP, Herlin P (2003) *Cytometry A* 56:37–45.